AGU PUBLICATIONS

Geophysical Research Letters

RESEARCH LETTER
10.1002/2015GL063506

Key Points:
- We made microstructure observations in the upper ocean during a rain event
- We observed thermohaline interfaces associated with double diffusion
- Double-diffusive mixing may occur in the tropics as a result of rain

Correspondence to:
B. Ward,
bward@nuigalway.ie

Citation:
Walesby, K., J. Vialard, P. J. Minnett, A. H. Callaghan, and B. Ward (2015), Observations indicative of rain-induced double diffusion in the ocean surface boundary layer, *Geophys. Res. Lett.*, *42*, 3963–3972, doi:10.1002/2015GL063506.

Received 22 FEB 2015
Accepted 20 APR 2015
Accepted article online 22 APR 2015
Published online 19 MAY 2015

Observations indicative of rain-induced double diffusion in the ocean surface boundary layer

K. Walesby[1], J. Vialard[2], P. J. Minnett[3], A. H. Callaghan[4], and B. Ward[1]

[1] AirSea Laboratory, School of Physics and Ryan Institute, National University of Ireland, Galway, Galway, Ireland, [2]Sorbonne Universités (UPMC, Université Paris 06)-CNRS-IRD-MNHN, LOCEAN/Institut Pierre Simon Laplace, Paris, France, [3]Rosenstiel School of Marine and Atmospheric Science, University of Miami, Miami, Florida, USA, [4]Scripps Institution of Oceanography, San Diego, California, USA

Abstract Double diffusion can result in the formation of thermohaline staircases, typically observed in the ocean interior. The observations presented here were acquired in the ocean surface boundary layer with the autonomous microstructure Air-Sea Interaction Profiler. An intense rain event (rainfall rates of up to 35 mm/h) resulted in cooler, fresher water (up to 0.15 practical salinity unit (psu) over the upper 7–10 m) overlaying warmer, saltier water, a situation potentially conducive to double-diffusive mixing. Although not as crisp as interfaces in the interior ocean because of elevated background mixing, a total of 303 thermohaline interfaces were detected within and at the base of the fresh layer, with mean changes in temperature (T) and salinity (S) across interfaces of 20×10^{-3}°C and 22×10^{-3} psu, respectively. These results call for new studies to disambiguate whether such interfaces are formed through double-diffusive mixing or shear instabilities and understand any long-term impacts on near-surface stratification.

1. Introduction

Ocean stratification is determined by a combination of the temperature (T) and salinity (S) structures, which can each contribute to stabilize or destabilize the fluid. Under certain circumstances an instability known as double diffusion can result [e.g., see *Schmitt*, 1994]. This instability is a product of the competing effects of temperature and salinity profiles on overall stratification, and the fact that heat and salinity possess very different molecular diffusion rates.

Double diffusion in seawater occurs when either warmer/saltier water overlies cooler/fresher water or vice versa. The latter situation results in the diffusive convection form of double diffusion, while the former leads to salt fingering. Salt fingering has been observed in various locations, including the western tropical North Atlantic [*Schmitt et al.*, 1987], the Mediterranean and Red Sea outflows [*Schmitt*, 1994], and the Tyrrhenian Sea [*Tait and Howe*, 1968]. Diffusive convection is typically seen at high latitudes [*Padman and Dillon*, 1987; *Sirevaag and Fer*, 2012]. Taken overall, large areas of the world's oceans are favorable to double diffusion [*You*, 2002].

Under strong double-diffusive conditions, stratified interfaces separated by thicker, well-mixed layers may develop [*Schmitt et al.*, 1987]. Since temperature and salinity vary vertically in a step-like manner, they have been termed thermohaline staircases. Such structures are the most dramatic signature of the action of double diffusion. A common feature of double-diffusive regions is their anomalously low values of density ratio (R_ρ), given by

$$R_\rho = \frac{\beta S_z}{\alpha T_z}, \tag{1}$$

where α and β are the thermal expansion and haline contraction coefficients, and T_z and S_z are the vertical temperature/salinity gradients. Salt fingering is associated with $0 < R_\rho < 1$, and $1 < R_\rho < 10$ is considered susceptible to diffusive convection [*Sirevaag and Fer*, 2012].

In the main thermocline, thermohaline staircases can have large-scale impacts since they represent areas of enhanced mixing. Two major field campaigns have investigated double diffusion in the Caribbean: Caribbean Sheets And Layers Transect [*Schmitt et al.*, 1987] and Salt Finger Tracer Release Experiment [*Schmitt et al.*, 2005].

These studies have found that staircases elevate the vertical mixing rate in the interior ocean by an order of magnitude, with implications for the global thermohaline circulation [*Zhang and Schmitt*, 2000].

Almost all thermohaline staircases have been reported either within or below the thermocline (depths of greater than 100–200 m). Other than a few cases of such features being observed close to melting icebergs [e.g., *Stephenson et al.*, 2011], there have not been any staircases reported within the ocean surface boundary layer (OSBL), defined as that layer which is directly affected by surface forcing [*Stevens et al.*, 2011], with its structure being established by the fluxes of energy, momentum, freshwater, and heat across the air-sea interface.

We present data from 170 profiles of the upper 40 m of the tropical Indian Ocean, spanning a single 18 h period. These data were collected using the Air-Sea Interaction Profiler (ASIP), a novel, microstructure profiler [*Ward et al.*, 2014; *Sutherland et al.*, 2014a]. During the period of observation, an intense rain event occurred. Since rainwater is both fresher and cooler than seawater [*McCulloch et al.*, 2012], the fluid configuration which arises from rain is favorable to diffusive convection. We observe numerous occurrences of simultaneous, high-gradient changes in salinity and temperature in the OSBL in our measurements and discuss their possible formation mechanism, including double diffusion. An overview of the observations collected is provided in section 2. Section 3 presents the microstructure data collected. A summary of the results can be found in section 4.

2. Observations

The observations presented here were obtained during the Cirene cruise, aboard the R/V *Suroît*. The Cirene experiment took place during January and February 2007 in the tropical Indian Ocean [*Callaghan et al.*, 2014]. In this region, known as the Seychelles-Chagos Thermocline Ridge, elevated sea surface temperatures and deep atmospheric convection are found, conducive to strong air-sea interactions under several climatically relevant phenomena such as tropical cyclones [*Vialard et al.*, 2008, 2009; *Cuypers et al.*, 2013]. This region is characterized by a shallow thermocline at 50 m (although it was unusually deep at 100 m in early 2007). Salinity increased with depth—from 34.4 at the surface to 34.8 at 100 m—due to the influence of frequent rain spells in this region.

2.1. Microstructure Measurements

The microstructure data presented here was collected on 15 February 2007 using ASIP. ASIP is an autonomous, vertically rising, microstructure profiler which operates within the upper ocean. ASIP is fully described in *Ward et al.* [2014] (although the version used here was a slightly modified design). During Cirene, ASIP's microstructure payload consisted of a shear probe (SPM-38), and a fast-response (7 ms) temperature sensor (FP07) provided by Rockland Scientific International. All sensors were sampled at 1024 Hz. The shear probes were used to estimate the rate of dissipation of turbulent kinetic energy (ϵ) following methods that have been established for several decades [e.g., *Osborn*, 1974]. More specific details on data processing can be found in *Callaghan et al.* [2014] and *Sutherland et al.* [2013].

2.2. Atmospheric Measurements

Since the atmospheric and oceanic boundary layers are coupled, gaining an understanding of the meteorological conditions which prevailed during the ASIP deployment is important. This was achieved by using the shipboard meteorological measurements made from the R/V *Suroît*, with air-sea fluxes calculated using the Tropical Ocean–Global Atmosphere Coupled Ocean-Atmosphere Response Experiment 3.0 algorithm [*Fairall et al.*, 2003].

Figure 1 shows time series of several meteorological and oceanic variables for the duration of the ASIP deployment. Figure 1a displays a time series of rain rate (RR) and wind friction velocity (u_*). These rain rate data indicate that a brief, weak rain event immediately preceded the ASIP deployment. Later, at approximately 0600 LT, a series of intense rain showers were experienced. These had largely passed by 0930 LT, although several weaker showers were recorded up to 1400 LT. The most intense showers saw rainfall rates of almost 35 mm/h. Rainwater was the dominant atmospheric forcing experienced during the ASIP deployment. The wind friction velocity began to increase from around 0200 LT, with further sharp increases in magnitude and variability concurrent with the onset of the intense rainfall at 0600 LT. After 0800 LT, the wind friction velocity reduced substantially, to below the level seen before the onset of rain.

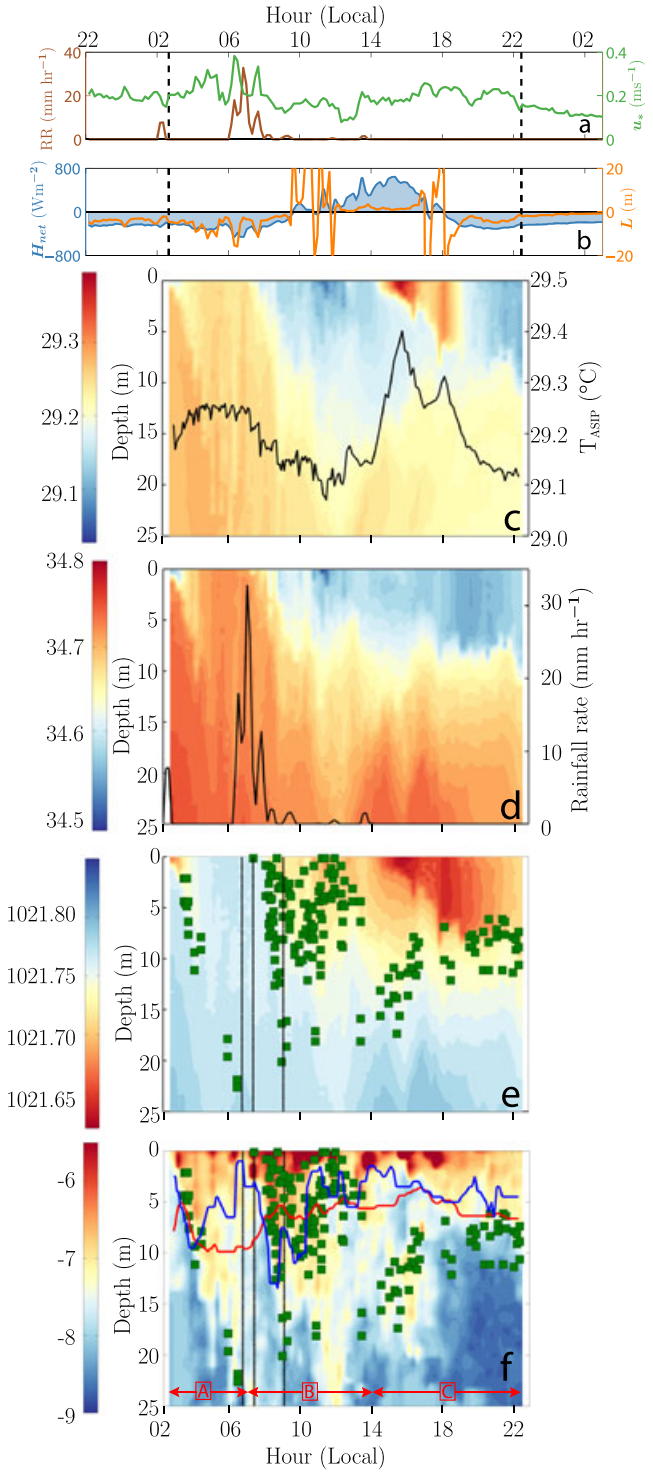

Figure 1. Time series of **a** rain rate and wind friction velocity, and **b** net heat flux and Obukhov length for the period of the ASIP deployment (15 February 2007). The vertical, dashed black lines indicate the relative timing of the first and last ASIP profiles in the deployment. Contour plots of **c** temperature, **d** salinity, **e** density and **f** ϵ are also shown (based on 170 ASIP profiles). The solid, black lines on **c** and **d** represent mean temperature of the upper 1 m for each ASIP profile and rainfall rate (as measured on the R/V *Suroît*), respectively. The green markers in **e** and **f** represent where thermohaline interfaces were detected within individual profiles. Also plotted on **e** and **f** are three vertical, black lines, indicating the time of three sample profiles (discussed in text). Red/blue lines in **f** indicate the depths of the mixed/mixing layers. The red arrows in **f** separate the timeseries into three periods, discussed in the text.

Figure 1b shows the net heat flux (H_{net}) recorded during the ASIP deployment. The sign convention for H_{net} is negative/positive when the heat flux is directed out of/into the ocean. The H_{net} record displays a typical diurnal variation, being positive during daytime and negative under nocturnal conditions. During the rain event, H_{net} increases in magnitude. This indicates the cooling effect of the rain on the ocean surface. The Obukhov length (L) is also plotted in Figure 1b and is defined as

$$L = -\frac{u_*^3}{\kappa B_0}, \tag{2}$$

where B_0 is the net buoyancy flux, $\kappa = 0.4$ is von Kármán's constant, and u_* is the friction velocity in water. Physically, L represents whether buoyancy- or shear-driven turbulence dominates the flow, taking positive/negative values for shear-/buoyancy-driven turbulence. The observations of L follow a typical diurnal cycle, being negative until 0930 LT (indicating instability), becoming positive during the daytime (driven by solar heating and having a magnitude of ~2 m between 1200 LT and 1700 LT), and then becoming negative again during the evening.

3. Results and Discussion

Figures 1c–1f display the evolution of the oceanic variables potential temperature (θ), salinity (S), density (ρ), and dissipation (ϵ), as observed by ASIP over the course of the deployment. These results indicate that rainfall exerted a striking impact on the OSBL. Figure 1c displays a contour plot of temperature measured by ASIP. The time series of mean temperature in the upper 1 m for each ASIP profile is also plotted. A clear cooling is seen in the θ data, around the time of the rain event. Rainwater is typically cooler than seawater by 5–10°C [*McCulloch et al.*, 2012]. It is argued that the cooling seen by ASIP is caused by a combination of the mixing of this rainwater with the warmer seawater, and enhanced evaporative cooling driven by the wind gusts during the rainy period. The cool, fresh layer associated with the rain that preceded the ASIP deployment remained until nighttime convection dispersed it. At ~0700 LT, rainfall was concurrent with a surface cooling of 0.15°C. This signal was seen down to depths of 20 m. At 1400 LT, a rapid surface warming is seen, caused by solar heating. This heating was masked until the afternoon because of the concurrent cooling from rainfall and associated cloud cover.

The rainwater also leaves a clear salinity signature (Figure 1d), evidenced by the rain event just prior to the beginning of the ASIP deployment. A freshening of ~0.2 practical salinity unit (psu) is seen at 0200 LT, although this was dispersed by nocturnal convection. After this, the salinity structure was relatively uniform, until the next rainfall event. Interestingly, although the rain sensors on the ship first detected precipitation at 0600 LT, ASIP does not sense a freshening and cooling until 0700 LT. Upon investigation, this discrepancy is attributed to the spatial separation between ASIP and the ship. This varied over the course of the deployment, from 0 km at the beginning of the deployment (when ASIP was launched from the ship) to 30 km later in the deployment. After 0700 LT, the salinity structure dramatically altered. The upper 10 m saw a freshening of at least 0.15 psu. This freshening was very close to estimates of the expected salinity change, given the observed rainfall. This indicates that rainfall is very likely the cause of the observed freshening. Salinity within this fresh layer was relatively uniform. Below this, there is a further 5–10 m thick layer in which the salinity transitions from the value within the freshwater pool to its background value below 25 m. Only very small salinity variations were seen by ASIP after the rain ceased (1400 LT).

As seawater density is determined by a combination of temperature and salinity, and rainwater is typically both fresher and cooler, this makes the resultant fluid configuration susceptible to double diffusion. The fresh pool formed by the rainfall had the effect of reducing the density of the near-surface waters by ~0.15 kg/m^3 (Figure 1e). This increased the static stability of the water column and suppressed vertical mixing. The diurnal warming between 1400 LT and 1800 LT further enhanced this stratification.

Figure 1f shows the variation in ϵ over the course of the deployment (this is discussed in the context of the rainfall events above). Between 0200 LT and 0600 LT, high dissipation levels (10^{-7} m^2 s^{-3}) were seen from the surface, down to a depth of 20 m (indicated as Period A in Figure 1f). This plume of elevated dissipation descended over time and was probably due to the earlier rainfall event. The ϵ seen within the plume exceeds by an order of magnitude that of the background level of nighttime convective dissipation (10^{-8} m^2 s^{-3}).

The rainfall after 0700 LT had a strong influence on ϵ, where there was an enhancement over the same depth range that the impact of cooling/freshening is seen (Period B). This increase in ϵ is attributed to a combination

of the increase in wind speed seen at this time, and the effect of raindrops on the vertical mixing within the OSBL [*Katsaros and Buettner*, 1969]. After the rainfall ceased, solar insolation warmed the surface and most of the turbulence was isolated within the upper 5–10 m (Period C). Below this well-defined, freshwater cap, ϵ reduced by more than 2 orders of magnitude.

Also plotted in Figure 1f are time series of mixed (MLD) and mixing (XLD) layer depths. These are defined as the depth at which the ρ/ϵ profiles first fall below a defined threshold. In this study, the MLD was calculated using a density threshold criterion of 0.03 kg m^{-3}, relative to the density at $z_r = 2.5$ m depth. The mixing layer depth was defined as the shallowest depth where ϵ first drops below a certain background level (10^{-7} m^2 s^{-3}). Vertical profiles of ϵ were processed into 0.5 m bins. To minimize the effect of temporal intermittency, these were then averaged into a six-profile running mean (equating to approximately a 30 min window). Further details on MLD/XLD can be found in *Sutherland et al.* [2014b]. The onset of rainfall exerts an interesting effect, with the freshening effect leading to the MLD becoming shallower. In contrast, the increase in near-surface dissipation seen at this time leads to a deepening for the XLD. After the rainfall ceases, both MLD and XLD assume broadly similar values.

The freshwater flux associated with the rainfall substantially altered the overall temperature and salinity structure. Figure 2 displays T, S, ρ, and R_ρ profiles from (i) just prior (0632 LT), (ii) just after (0711 LT), and (iii) 2 h after the onset of rain (0854 LT). In the 0711 LT profile, a sharp, linear freshening and cooling is seen, confined to the upper 1 m of the profile. By the 0854 LT profile, a series of thermohaline interfaces have formed, extending over the upper 20 m. Such features were present in many ASIP profiles after the onset of rain.

While such staircases have been observed before [e.g., *Schmitt*, 1994], they have normally been seen at depths $z > 100$ m, where the waters are more quiescent. Such staircases have been associated with double-diffusive activity. Double diffusion could also explain the staircases seen here, since the postrainfall fluid configuration was favorable in this regard. This would represent a newly found regime for the occurrence of double diffusion in the ocean. The deformation of the interfaces from the crisp vertical mixed layer to horizontal interface pattern seen in the interior ocean is attributed to the much elevated background mixing level within the OSBL.

However, it is not inconceivable that other processes could also result in the formation of these features. It is possible that the highly heterogeneous nature of rainfall—resulting in spatially heterogeneous, near-surface freshening—could combine with fine-scale, vertical shear to form thermohaline staircase-like structures. Since it is not possible to use our data set to absolutely discriminate between these processes, we simply note here this possible alternative. As can be seen from Figure 2d, however, the interfaces in the sample profile all fall within the range favorable for diffusive convection. This was true of almost every interface identified. Taken together with the fact that the rainwater flux established a fluid configuration associated with double diffusion, and some time afterward a thermohaline staircase was seen to form (which is classically associated with double diffusion), this lends credence to the view that double diffusion is an important mechanism at work in this case.

The area occupied by thermohaline staircases is controlled by the competition between turbulent mixing and double diffusion. Numerical experiments have shown that when diapycnal mixing is predominantly double diffusive, staircases spread throughout the model domain [*Radko et al.*, 2014]. When the strengths of double-diffusive and turbulent mixing are comparable, staircases are more localized. When the turbulent diffusivity exceeds that of double diffusion, staircases do not form. In the present case, thermohaline interfaces are seen to form within the OSBL—where turbulent mixing undoubtedly dominates double diffusion. Although it is extremely difficult to track individual interfaces using a vertical profiler, the lifetimes of these are thought to be very limited (at least within the upper 10 m).

Within the interior ocean, thermohaline interfaces have been observed to have an impact upon ϵ structure [*St. Laurent and Schmitt*, 1999]. In this case, the strong vertical variation in ϵ within the OSBL, combined with the transient nature of the interfaces, meant that the effect of these on ϵ profile was unclear. The vertical scale of these interfaces was typically less than a meter, and several were found within the uppermost 10 m. This perhaps explains why they have not been observed before—most microstructure profilers are incapable of measuring this part of the water column.

In order to characterize the thermohaline interfaces, a quantitative method for identifying them was developed. Although manual identification is one approach, there are evident improvements in robustness when an automated method is used. The method developed here was based upon that developed by *Sirevaag and*

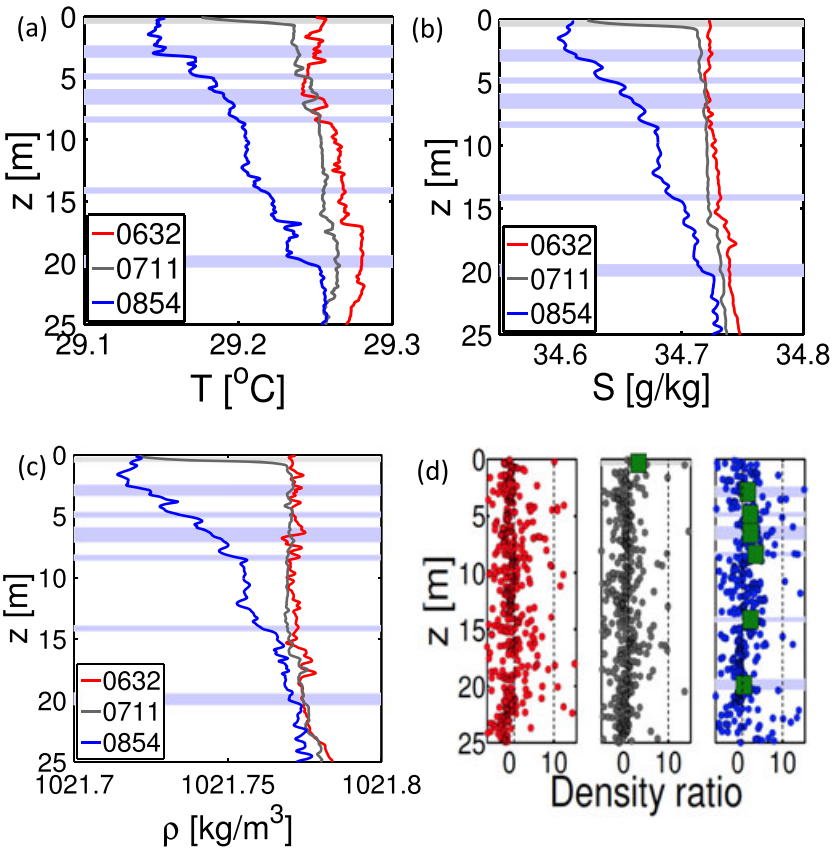

Figure 2. (a) Temperature, (b) salinity, and (c) density structures, as measured during three representative profiles. These profiles were measured at 0632 LT (red), 0711 LT (grey), and 0854 LT (blue) and demonstrate how the water column was substantially modified by the freshwater input, ultimately leading to the formation of thermohaline interfaces. Identified interfaces in the 0711/0854 LT profiles are highlighted with grey/blue stripes. (d) R_ρ structure for the three profiles (same color convention). The circular markers represent R_ρ calculated using subsequent measurements throughout the profile. The green, square markers indicate R_ρ calculated using a bulk approach for each identified interface, taking the *T*/*S* values at the beginning/end of each interface. The vertical, dashed lines indicate the limits of the diffusive convection regime.

Fer [2012] for identifying double-diffusive staircases in the Arctic. Whereas *Sirevaag and Fer* [2012] studies staircases at depths of several hundred meters, the staircases presented here were observed within the more turbulent OSBL. This environment presents additional challenges for the method. Of particular note is the deforming effect of increased shear levels on the crispness of the interfaces. The ASIP temperature and salinity data were processed at 1 cm vertical resolution. Following *Schmitt et al.* [1987], a simultaneous change in the local temperature and salinity gradients was used as the signature of a thermohaline interface. For each profile, background temperature and salinity gradients were calculated, based on a 250-point running mean (equivalent to a vertical window of 2.5 m). Once these background gradients had been established, the local gradient (based upon subsequent measurements) was compared against these. The temperature and salinity jumps associated with thermohaline interfaces were defined as occurring when this local temperature and salinity gradient exceeded the magnitude of the background temperature and salinity gradients. Where these background temperature and salinity gradients were both positive/negative, the staircase was associated with the possible action of salt finger/diffusive convection.

Several developments to this method yielded improved performance. First, a minimum local temperature gradient within interfaces of 20×10^{-3}°C m^{-1} was specified. For salinity, no minimum threshold was specified, but the criterion was that the temperature/salinity gradients had to have the same sign. Second, the method would sometimes identify two separate interfaces where a single, continuous one existed. This was addressed by merging interfaces when they were separated by only a small vertical distance (here 40 cm). Finally, a number of spurious interfaces were identified. When an interface contained fewer than 40 measurements,

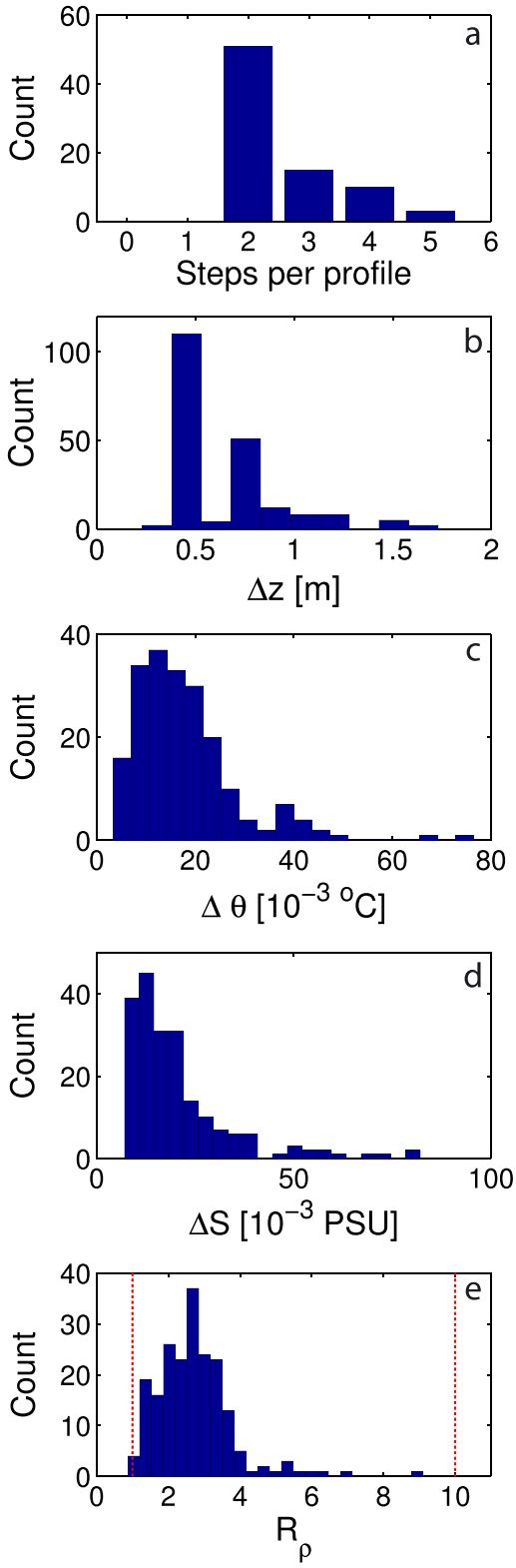

Figure 3. Histograms of key staircase properties, as found by the thermohaline interface method: (a) number of interfaces per profile, (b) height of thermohaline interfaces, (c) $\Delta\theta$ across interface, (d) ΔS across interface, and (e) R_ρ within interfaces. The red, dashed lines in Figure 3e indicate the upper and lower limits of R_ρ for the diffusive convection regime.

it was discarded. This method was tested using the ASIP data, and it proved an efficient method of identifying thermohaline interfaces. The merit of each parameter described above and the value it should take were investigated before deciding on those detailed.

The above method was applied to all ASIP profiles, and the interface locations are marked in Figures 1e and 1f. The spatial distribution of these presents a rather confused picture initially, which becomes more coherent later. It should be remembered that a small rain event preceded this ASIP deployment. This resulted in some surface freshening, although this was largely mixed away during nighttime convection. This rainfall event may have triggered the thermohaline interfaces seen before 0400 LT. Typically, nocturnal mixing disrupted the staircase, although some isolated thermohaline interfaces remained between 0400 and 0800 LT. The new rainwater flux, after 0800 LT, triggered the formation of many thermohaline interfaces in the upper 10 m. Between 0800 and 1400 LT, these interfaces were observed both within the uniformly fresh pool, where they are concentrated at the base of the mixing layer, as well as immediately below this in the interface between the fresh pool and the underlying water. After 1300 LT, the freshening and cooling trend seen at the surface ceased. Up to this point, the effect of the diurnal solar heating had been masked by the effect of the relatively cold rainwater and cloud cover associated with this precipitation. After 1400 LT, however, a solar-induced warming signal is seen. This increased the temperature of the upper 5 m without altering the salinity, shifting this part of the water column out of the double-diffusive regime and into the doubly stable regime. Thereafter, no thermohaline interfaces were observed within this upper 5 m layer, although thermohaline interfaces remained in the transition region separating the fresh and salty layers (5–25 m). Where interfaces were identified in the sample profiles, a bulk measure of R_ρ was plotted in Figure 2d. These values were calculated using the temperature and salinity at the beginning and ends of each interface. These show that the conditions within these interfaces were favorable to double diffusion.

In total, 303 thermohaline interfaces were identified. By altering T/S structure from a linear to a stepped form (with high-gradient interfaces separated by well-mixed layers), double diffusion can act to enhance vertical transport within

the water column. In order to investigate the properties of the thermohaline staircases further, we restricted our subsequent analysis to only those profiles containing multiple interfaces. This reduced the total number of interfaces seen to 202, with on average 2.6 interfaces detected per profile. The mean ΔT and ΔS across each thermohaline interface was $(18 \pm 11) \times 10^{-3}$°C and $(20 \pm 13) \times 10^{-3}$ psu, respectively. The mean value for R_ρ, within each interface was found to be (2.7 ± 1.1). This places these staircases firmly within the diffusive convection favorable regime. Assuming these interfaces were caused by double diffusion, their impact on heat flux ($F_{H_{K90}}$) was estimated for each interface using the "4/3 flux law" inferred from laboratory studies [*Kelley*, 1990]:

$$F_{H_{K90}} = \rho c_p \frac{C}{\alpha} \left(\frac{g \kappa_T^2}{\nu} \right)^{\frac{1}{3}} (\alpha \Delta T)^{\frac{4}{3}}, \tag{3}$$

where ρ is the density, c_p is the specific heat, g is the constant of gravity, κ_T is the thermal diffusivity, ν is the kinematic viscosity, and ΔT is the temperature difference across the interface. More recently, *Flanagan et al.* [2013] demonstrated that the heat transport in the ocean is likely higher than that indicated by (3) by as much as a factor of 2. The physical basis for this revision is because the rigid boundaries which are present in laboratory experiments are not found in the ocean. The flux scale factor, C, was estimated using the empirical relation [*Kelley*, 1990]:

$$C = 0.0032 e^{\frac{4.8}{R_\rho^{0.72}}}, \tag{4}$$

where R_ρ is the density ratio across the interface. This parameterization yielded an arithmetic mean for all interfaces of (-0.25 ± 0.33) W m^{-2} (upward). While this mean flux is comparable to those reported for previous interfaces [e.g., *Sirevaag and Fer*, 2012], these other staircases were seen at much greater depths (>100 m), where the turbulent mixing rate was substantially lower. Within the OSBL, any contribution from double diffusion to the overall heat flux would be extremely small compared to that due to turbulence. The mean value quoted above is smaller than the associated standard deviation because the distribution is long tailed. The heat flux for each individual interface detected was negative.

Figure 3 displays histograms of these same properties for multi-interface profiles. Of particular note is the distribution of R_ρ (Figure 3e). Diffusive convection becomes more vigorous as R_ρ approaches 1 from above. The vast majority of the interfaces identified are thus found under conditions which are highly favorable to diffusive convection. This provides further support that double diffusion could be an important mechanism leading to the formation of the thermohaline interfaces. Clearly, since the staircases reported here were observed in a very different environment to most previously seen, no directly comparable measurements exist in the literature. Interestingly, diffusive convection is typically seen at high latitudes and below the thermocline [*Padman and Dillon*, 1987; *Sirevaag and Fer*, 2012]. These observations of possible diffusive convection in near-surface, tropical waters are, therefore, unexpected. At the time of writing, and to the best of the authors' knowledge, the thermohaline interfaces presented here are the first identified as possibly being formed due to the effect of rainfall. However, the $\Delta T_{\text{interface}}$ and $\Delta S_{\text{interface}}$ seen here are very similar to those reported by, for example, *Timmermans et al.* [2008]. Correspondingly, their estimate of heat flux was similar (0.22 W m^{-2}). It must be remembered, however, that the staircases reported by *Timmermans et al.* [2008] were observed at much greater depths (200–300 m). At such depths, the waters are more quiescent. This means that the staircases are both less disrupted by the effects of turbulence and likely to make a larger proportional contribution to the overall heat flux. Those staircases reported in *Timmermans et al.* [2008] were also much more mature, having existed for decades (rather than only several hours in this case). However, the newly formed staircases reported here means that the staircase formation process has a definite start time—the time of the onset of rainfall. The approximate volume of freshwater forcing can also be estimated. This open-ocean, staircase-forming event may thus be of interest to the modeling community as a case study for staircase formation.

4. Conclusions

This study presents an investigation into the effect of rainfall on temperature and salinity structures within the OSBL. A total of 170 microstructure profiles were acquired in the tropical Indian Ocean, spanning an 18 h period. The impacts of an intense rain event were observed. ASIP data demonstrated that the freshwater flux had a profound effect on T/S structure over the upper 20 m. Many individual profiles contained

concurrent temperature and salinity interfaces. These thermohaline interfaces are typically associated with double-diffusive activity. However, interleaving of different water masses—associated with the combination of fine-scale vertical shear and the highly heterogeneous nature of rainfall—could also possibly lead to the formation of these thermohaline interfaces. It was not possible to use our observations to absolutely discriminate between these mechanisms, but it is hoped that laboratory and numerical experiments may provide insights into the mechanisms at play. The fact that a thermohaline staircase was seen to form after rainwater set up a double-diffusive favorable fluid configuration points toward the double-diffusive mechanism at least being plausible. When R_ρ was diagnosed, almost all 303 identified interfaces were seen to fall within the diffusive convection regime, lending further credence to the double-diffusive explanation. While these signatures are suggestive of double diffusion, alternative mechanisms may be involved, which warrant further observational investigations and modeling studies.

A method was developed for identifying these within the ASIP data set, showing that such interfaces were widespread both during and after rainfall. After the rain ceased, diurnal heating pushed the upper 5 m of the water column out of the double-diffusive regime, and no more interfaces were seen here. However, many interfaces were identified at greater depths, right up to the end of the deployment. The ubiquitous nature of mesoscale convective systems in this region means that the conditions which resulted in the formation of these interfaces are likely to be seen frequently at the bottom of the mixed layer in the tropics after strong rain spells. However, the contribution of double-diffusive mixing to overall mixing is probably small, since the heat fluxes it induces are at least an order of magnitude smaller than those associated with background turbulence.

Observations were also made of the dissipation rate of turbulent kinetic energy ϵ. Interestingly, an increase in ϵ was seen over the upper 5–10 m during the rain-affected periods. This is likely due to increased wind mixing at this time, driving shear, and inertial instabilities. After this, there was evidence that the freshwater pool trapped much of the turbulence within it, suppressing mixing below it. This resulted in a change in ϵ across the freshwater puddle interface of more than 2 orders of magnitude.

To the best of our knowledge, these are the first observations of thermohaline interfaces triggered by rainfall. This is attributed to the fact that most microstructure profilers are incapable of measuring the upper 10 m of the water column—precisely that part of the water column most affected by air-sea fluxes. It is anticipated that direct numerical simulations and modeling studies, laboratory experiments, and field observations will provide further insights into processes resulting in the observed structures, required to properly understand the roles of turbulence and double diffusion close to rain-induced, freshwater puddles.

Acknowledgments

The authors are grateful for funding support from the European Space Agency (contract 4000102925/11/I-AM), the Irish Research Council (grant EPSPD/2011/218), and the Office of Naval Research (award N62909-14-1-N296). We thank the captain and crew of the R/V *Suroît* for their help and support during the campaign. Any requests concerning the data in this paper should be directed to the corresponding author.

The Editor thanks two anonymous reviewers for their assistance in evaluating this paper.

References

Callaghan, A. H., B. Ward, and J. Vialard (2014), Influence of surface forcing on near-surface and mixing layer turbulence in the tropical Indian Ocean, *Deep Sea Res., Part I*, *94*, 107–123, doi:10.1016/j.dsr.2014.08.009.

Cuypers, Y., X. Le Vaillant, P. Bouruet-Aubertot, J. Vialard, and M. J. Mcphaden (2013), Tropical storm-induced near-inertial internal waves during the Cirene experiment: Energy fluxes and impact on vertical mixing, *J. Geophys. Res. Oceans*, *118*, 358–380, doi:10.1029/2012JC007881.

Fairall, C., E. F. Bradley, J. Hare, A. Grachev, and J. Edson (2003), Bulk parameterization of air-sea fluxes: Updates and verification for the COARE algorithm, *J. Clim.*, *16*(4), 571–591.

Flanagan, J. D., A. S. Lefler, and T. Radko (2013), Heat transport through diffusive interfaces, *Geophys. Res. Lett.*, *40*, 2466–2470, doi:10.1002/grl.50440.

Katsaros, K., and K. J. Buettner (1969), Influence of rainfall on temperature and salinity of the ocean surface, *J. Appl. Meteorol.*, *8*(1), 15–18.

Kelley, D. E. (1990), Fluxes through diffusive staircases: A new formulation, *J.Geophys.Res.*, *95*(C3), 3365–3371.

McCulloch, M., P. Spurgeon, and A. Chuprin (2012), Have mid-latitude ocean rain-lenses been seen by the SMOS satellite?, *Ocean Modell.*, *43*, 108–111.

Osborn, T. R. (1974), Vertical profiling of velocity microstructure, *J. Phys. Oceanogr.*, *4*(1), 109–115.

Padman, L., and T. M. Dillon (1987), Vertical heat fluxes through the Beaufort Sea thermohaline staircase, *J. Geophys. Res.*, *92*(C10), 10,799–10,806.

Radko, T., A. Bulters, J. Flanagan, and J.-M. Campin (2014), Double-diffusive recipes. Part I: Large-scale dynamics of thermohaline staircases, *J. Phys. Oceanogr.*, *44*(5), 1269–1284.

Schmitt, R. W. (1994), Double diffusion in oceanography, *Annu. Rev. Fluid Mech.*, *26*(1), 255–285.

Schmitt, R. W., H. Perkins, J. Boyd, and M. Stalcup (1987), C-salt: An investigation of the thermohaline staircase in the western tropical North Atlantic, *Deep Sea Res., Part A*, *34*(10), 1655–1665.

Schmitt, R. W., J. R. Ledwell, E. T. Montgomery, K. L. Polzin, and J. M. Toole (2005), Enhanced diapycnal mixing by salt fingers in the thermocline of the tropical Atlantic, *Science*, *308*, 685–688.

Sirevaag, A., and I. Fer (2012), Vertical heat transfer in the Arctic Ocean: The role of double-diffusive mixing, *J. Geophys. Res.*, *117*, C07010, doi:10.1029/2012JC007910.

Stephenson, G. R., J. Sprintall, S. T. Gille, M. Vernet, J. J. Helly, and R. S. Kaufmann (2011), Subsurface melting of a free-floating Antarctic iceberg, *Deep Sea Res., Part II*, *58*(11), 1336–1345.

St. Laurent, L., and R. W. Schmitt (1999), The contribution of salt fingers to vertical mixing in the North Atlantic tracer release experiment*, *J. Phys. Oceanogr.*, *29*(7), 1404–1424.

Stevens, C., B. Ward, C. S. Law, and M. Walkington (2011), Surface layer mixing during the SAGE ocean fertilization experiment, *Deep-Sea Res.*, *58*, 776–787.

Sutherland, G., K. H. Christensen, and B. Ward (2013), Wave-turbulence scaling in the ocean mixed layer, *Ocean Sci.*, *9*, 597–608, doi:10.5194/os-9-597-2013.

Sutherland, G., K. H. Christensen, and B. Ward (2014a), Evaluating Langmuir turbulence in the oceanic boundary layer, *J. Geophys. Res.*, *119*, 1899–1910, doi:10.1002/2013JC009537.

Sutherland, G., G. Reverdin, L. Marié, and B. Ward (2014b), Mixed and mixing layer depths in the ocean surface boundary layer under conditions of diurnal stratification, *Geophys. Res. Lett.*, *41*, 8469–8476, doi:10.1002/2014GL061939.

Tait, R., and M. Howe (1968), Some observations of thermo-haline stratification in the deep ocean, *Deep Sea Res.*, *15* (3), 275–280, doi:10.1016/0011-7471(68)90005-3.

Timmermans, M.-L., J. Toole, R. Krishfield, and P. Winsor (2008), Ice-tethered profiler observations of the double-diffusive staircase in the Canada basin thermocline, *J. Geophys. Res.*, *113*, C00A02, doi:10.1029/2008JC004829.

Vialard, J., G. Foltz, M. McPhaden, J.-P. Duvel, and C. de Boyer Montégut (2008), Strong Indian Ocean sea surface temperature signals associated with the Madden-Julian Oscillation in late 2007 and early 2008, *Geophys. Res. Lett.*, *35*, L19608, doi:10.1029/2008GL035238.

Vialard, J., et al. (2009), Cirene: Air-sea interactions in the Seychelles-Chagos thermocline ridge region, *Bull. Am. Meteorol. Soc.*, *90*, 45–61, doi:10.1175/2008BAMS2499.1.

Ward, B., T. Fristedt, A. H. Callaghan, G. Sutherland, X. Sanchez, J. Vialard, and A. ten Doeschate (2014), The Air-Sea Interaction Profiler (ASIP): An autonomous upwardly rising profiler for microstructure measurements in the upper ocean, *J. Atmos. Oceanic Technol.*, *31*, 2246–2267, doi:10.1175/JTECH-D-14-00010.1.

You, Y. (2002), A global ocean climatological atlas of the Turner angle: Implications for double-diffusion and water-mass structure, *Deep Sea Res., Part I*, *49*(11), 2075–2093.

Zhang, J., and R. W. Schmitt (2000), The impact of salt fingering on the thermohaline circulation under mixed boundary conditions*, *J. Phys. Oceanogr.*, *30*(6), 1223–1231.